

Nanoscale

Accepted Manuscript



This is an *Accepted Manuscript*, which has been through the Royal Society of Chemistry peer review process and has been accepted for publication.

Accepted Manuscripts are published online shortly after acceptance, before technical editing, formatting and proof reading. Using this free service, authors can make their results available to the community, in citable form, before we publish the edited article. We will replace this *Accepted Manuscript* with the edited and formatted *Advance Article* as soon as it is available.

You can find more information about *Accepted Manuscripts* in the [Information for Authors](#).

Please note that technical editing may introduce minor changes to the text and/or graphics, which may alter content. The journal's standard [Terms & Conditions](#) and the [Ethical guidelines](#) still apply. In no event shall the Royal Society of Chemistry be held responsible for any errors or omissions in this *Accepted Manuscript* or any consequences arising from the use of any information it contains.

ARTICLE

Periodic Layered Inverse Micelle Multilayers with Tunable Photonic Band Gap: Fabrication and Application in Dye-Sensitized Solar Cells

Yoon Hee Jang and Dong Ha Kim*

Cite this: DOI:
10.1039/x0xx00000xReceived 00th January 2012,
Accepted 00th January 2012

DOI: 10.1039/x0xx00000x

www.rsc.org/

Periodic organic-inorganic multilayer films are constructed by stepwise alternate build-up of UV-stabilized poly(styrene-*block*-vinylpyridine) block copolymer inverse micelle and poly(styrene-*block*-ethylene oxide) block copolymer layers containing inorganic moieties at the polar core blocks. The layered block copolymer inverse micelle films show strong reflective color and well-defined photonic stop bands in the entire wavelength regions from visible to near IR, which can be fine-tuned by controlling the inner architectures, i.e., periodic size of layered structure. The layered block copolymer films are integrated into the back-side of the counter electrodes as light reflection layer and thereby enhancement ratio of ~11 % in the cell efficiency is achieved, which can be attributed to the increased light harvesting by sensitized dye molecules. Tailoring the inner structure of the photonic band gap multilayers, the wavelength of reflected light can be adjusted to the wavelength of dye absorption, leading to a noticeable enhancement in photocurrent and power conversion efficiency.

Introduction

Since the environmental issues regarding global warming consistently come to the fore, a need for generating renewable energies by photovoltaic technologies has been emphasized all over the world. As third-generation photovoltaic system, dye-sensitized solar cells (DSSCs) have gained tremendous interest as potential photovoltaic devices for solar to energy conversion owing to its relatively low fabrication cost and high power conversion efficiency (PCE).¹⁻⁴ The DSSCs technologies have made rapid progress in recent years through finding new materials and structure innovations.⁵ As one of the breakthroughs, the solution-processable organic-inorganic hybrid perovskites-absorber based solar cells exhibit superior efficiency of approximately 15 percent under standard AM1.5G illuminations by virtue of absorbing over a broad spectral range of light, from visible to near infrared (near-IR) wavelengths.⁶

Judging by this advance, the incident photon management, which is one more way to increase the PCE in solar cells, is a crucial factor to enhance the light harvesting efficiency (LHE). The many attempts for enhancing the LHE in DSSCs system have been executed in diverse directions: (1) Light scattering: the large sized colloid particles were incorporated into the cell as a diffuse scattering layer to increase the effective optical path length by photon scattering.⁷⁻⁹ More recently, hierarchically structured building blocks have received considerable attention

as photoanodes in DSSCs due to their unique structure effect of higher dye loading via large surface area, superior light scattering ability, and fast charge transport, which achieve a synergy effect.¹⁰⁻¹² (2) Enhanced surface plasmon resonance (SPR) fields: SPR supported by the use of metallic nanostructures led to enhanced light absorption and photocurrent generations.¹³⁻¹⁶ (3) Light trapping: conventional way for achieving the light trapping is the use of geometrical optics, such as mirror and surface grating in thin film silicon solar cells,^{17,18} or a new approach to successfully enhance the light trapping includes the introduction of optical wave such as photonic crystal. In particular, it has been reported that various dimensional and types of photonic crystals can be simply introduced in DSSCs to enhance the LHE in the specific range of wavelength.¹⁹⁻²² Colodrero et al. fabricated nanoparticle-based porous 1-dimensional (1D) photonic crystals, which were coupled to a dye-sensitized TiO₂ electrode. As a result, the PCE is enhanced by 18 % (from 3.9 % to 4.6 %) due to amplified light absorption at photonic band gap frequency.²³ Guldin et al. prepared 3-dimensional (3D) TiO₂ inverse opal and integrated into mesoporous TiO₂ underlayer as an optically active 3D photonic crystal overlayer.²⁴ The integration of photonic crystal increases the photogenerated current by 9.3 % (from 4.3 mA/cm² to 4.7 mA/cm²) and broadens the light harvesting capability of DSSCs. A novel structure, consisting of a thick TiO₂ nanoparticle layer and a thin TiO₂ nanotube photonic

crystal, were designed by Guo *et al.* The maximum enhancement in PCE of 39.5 % (from 4.99 % to 6.96 %) was achieved by best matching of its reflectance maximum to dye absorption.²⁵ Lee and co-workers developed solid-state DSSCs fabricated with Bragg stack-functionalized counter electrode, which was prepared via alternating deposition of organized mesoporous TiO₂ and colloidal SiO₂ layers on the non-conducting side of the counter electrode. LHE and photocurrent was maximized by reflecting unabsorbed photons back to the device, resulting in an enhancement of PCE by 22.2 % (from 5.4 % to 6.6 %).²⁶

The unique property of block copolymer (BCP) self-assembly has enabled self-assembled BCP structures to be exploited as promising platforms for inventing various dimensional photonic crystals. More specifically, the periodic size and shape of photonic crystals can be simply controlled by modulating the self-assembly parameters such as volume fractions of the constituent blocks, segment size, and the strength of interaction between the blocks.²⁷⁻²⁹ Kang *et al.* generated the robust photonic crystal gels by swelling the poly(styrene-*block*-2-vinylpyridine) (PS-*b*-P2VP) BCP with modest-molecular weight.³⁰ The swollen PS-*b*-P2VP film exhibited stop bands in the visible regime and fixed by infiltrating SiO₂ into the polar P2VP domains. In this study, we introduce a new class of organic/inorganic 1D photonic crystals exhibiting stop bands in the specific wavelength range, which was created by stepwise layer-by-layer deposition of UV-crosslinked BCP inverse micelle layers. The simple yet novel 1D layered BCP films have been introduced into the back-side of the counter electrodes as light reflector in DSSCs system.

Experimental

Materials.

All chemicals were used as provided without further purification. Poly(styrene-*block*-2-vinylpyridine) (PS-*b*-P2VP, $M_n^{PS} = 50 \text{ Kg mol}^{-1}$, $M_n^{P2VP} = 16.5 \text{ Kg mol}^{-1}$, $M_w/M_n = 1.09$), poly(styrene-*block*-4-vinylpyridine) (PS-*b*-P4VP, $M_n^{PS} = 41 \text{ Kg mol}^{-1}$, $M_n^{P4VP} = 24 \text{ Kg mol}^{-1}$, $M_w/M_n = 1.09$), and poly(styrene-*block*-ethylene oxide) (PS-*b*-PEO, $M_n^{PS} = 10 \text{ Kg mol}^{-1}$, $M_n^{PEO} = 11.5 \text{ Kg mol}^{-1}$, $M_w/M_n = 1.09$) BCPs were purchased from Polymer Source Inc. and used as received. 1,4-Dioxane, concentrated hydrochloric acid (HCl, 37%), and isopropyl alcohol (IPA) were purchased from Daejung Chemicals & Metals Co., Ltd. and used without further purification. Titanium tetraisopropoxide (TTIP) and silver nitrate (AgNO₃) was purchased from Sigma Aldrich.

Preparations of Block Copolymer Inverse Micelle Solutions.

S4VP was dissolved in toluene and stirred at 70 °C for 2 hours to yield the clear solution of inverse micelles composed of a PS corona and a P4VP core with a concentration of 1 wt% or 2 wt%. A homogeneous solution of SEO in 1,4-Dioxane with a concentration of 1 wt% was prepared by stirring at room-temperature for 2 hours. As prepared TiO₂ sol-gel precursor

(TTIP : HCl : IPA = 0.71 g : 0.25 g : 5 mL) was mixed with SEO solution (60/40 vol%) and stirred vigorously for overnight.³¹

Fabrications of 1-Dimensional Layered Block Copolymer Multilayer.

First layer of S4VP was prepared from 1 wt% or 2 wt% S4VP solution on solid substrate by spin coating at 1000 rpm for 60 seconds and stabilized by exposing to UV light with a wavelength of 254 nm with a dose of 25 J cm⁻² (XX-15S; UVP Inc.) for 1 hour in vacuum. Then, second layer of SEO/TiO₂ was prepared from 1 wt% SEO/TiO₂ (60/40 vol%) solution on stabilized S4VP layer by spin coating at 1500 rpm for 60 seconds and exposed to UV light ($\lambda = 254 \text{ nm}$) under vacuum condition for 1 hour. To fabricate multilayered BCP structures, the procedures described above were repeated.

Fabrication of Dye-Sensitized Solar Cells.

WORKING ELECTRODE FABRICATION. Fluorine-doped tin oxide (FTO, 2.2 mm thick and sheet resistance of 6 - 9 Ohms/sq.) glass pieces were washed by sonication in acetone, IPA, and distilled water baths sequentially for half an hour. nanocrystalline TiO₂ (nc-TiO₂) nanoparticles prepared from Degussa P25, ethyl cellulose, α -terpineol, and ethanol were deposited on FTO glass substrate by using doctor blade and heated at 125 °C for 6 minutes and 500 °C for 1 hour.³² Prior to dye adsorption, sintered nc-TiO₂ film was treated by TiCl₄ (40 mM) and exposed to oxygen plasma for 10 minutes under a given condition of 50 sccm (standard cubic centimeter per minute) and 100 W. Subsequently, nc-TiO₂ film was sensitized by the ruthenium dye (cis-diisothiocyanato-bis(2,2'-bipyridyl-4,4'-dicarboxylato) ruthenium(II) bis(tetrabutylammonium), N-719, Solaronix) by soaking in 0.2 mM dye/ethanol solution for 24 hours.

COUNTER ELECTRODE FABRICATION. According to the fabrication method, the 1D layered BCP structures were fabricated on the opposite side of platinum (Pt, average thickness of 2.8 nm) sputtered FTO glass. Working and counter electrodes were assembled by insertion of spacer (50- μm -thick hot-melt sealing foil, SX1170-25, Solaronix) and an ionic liquid electrolyte (0.60 M BMIM-I, 0.03 M I₂, 0.50 M TBP, and 0.10 M GTC in acetonitrile/valeronitrile 85/15 (v/v) (No. ES-0004), purchased from io.li.tec (Germany), was then injected to small gap between two electrodes driven by capillary force. The current density versus voltage (*J*-*V*) response of the DSSCs was measured under simulated AM 1.5 G illuminations intensity of 100 mW/cm² using a POLARONIX® K3000 Solar Cell I-V Measurement System. The exposed photoactive area for DSSCs was 0.25 cm².

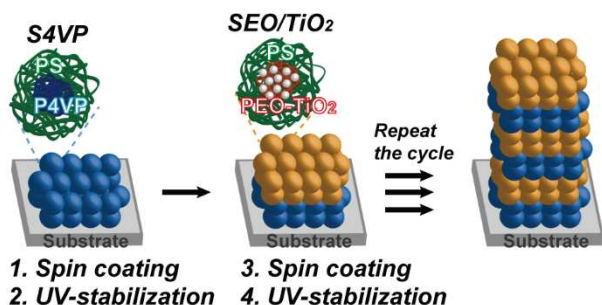
Instruments and Characterizations.

Atomic force microscopy (AFM) images were obtained using a Dimension 3100 scanning force microscope in tapping mode (Digital Instrument). Cross-sectional scanning electron microscopy (SEM) images were obtained by JEOL JSM6700-F. Spectroscopic ellipsometry (SEMG-1000, Nanoview Co.),

which is operated at an incidence angle of 70° with halogen light source of wavelength range from 350 to 850 nm, was used to measure the refractive indices and thickness of each layer. UV-Vis absorption or transmittance spectra were plotted by UV-Vis-NIR spectrometer (Cary 5000, Varian Inc.).

Results and discussion

Organic/inorganic hybrid periodic layered structures, which were composed of polymer and TiO_2 , were prepared by stepwise build-up of photo-crosslinkable PS-*b*-P4VP (denoted as S4VP) and PS-*b*-PEO (denoted as SEO) containing TiO_2 sol-gel precursor in an alternating fashion. The whole fabrication process for 1D layered structure with well-defined periodicity assisted by BCP layer-by-layer assembly was schematically illustrated in Scheme 1. As shown in Scheme 1, the one cycle was comprised of four-stages: The S4VP homogeneous solution was spin coated onto a solid substrate to develop thin BCP inverse micelle film (stage 1). The S4VP inverse micelle layer was subsequently exposed to UV light to stabilize the film (stage 2).³³⁻³⁵ The relatively thick second layer having TiO_2 arrays was constructed by consecutive adsorption from a SEO solution containing 40 vol% TiO_2 sol-gel precursor on S4VP layer (stage 3) followed by UV-stabilization (stage 4). The formation of 1D stacked multilayer films was achieved by repeating the stages from 1 to 4.



Scheme 1. Schematic illustration for hybrid layered nanostructures fabricated by stepwise layer-by-layer assembly of UV-stabilized BCP inverse micelles.

The topographies of each constituting layer were investigated by atomic force microscopy (AFM). As shown in Fig. 1(a), the upper and lower parts display surface morphologies of 1 wt% S4VP layers and SEO/ TiO_2 (60/40 vol%) layers after UV exposure for 1 hour, respectively. With the increase in the number of layers, the surface texture of each layer was conserved without any alterations such as collapse and aggregation while roughness was slightly increased. Stepwise deposition of stabilized BCP films was also confirmed by cross-sectional scanning electron microscopy (SEM). In Fig. 1(b), the ten-layers consisting of the relatively thin S4VP layers and thick SEO/ TiO_2 layers were observed, indicating that the hybrid BCP films were successfully stacked through UV-stabilization and subsequent layer deposition. However, the S4VP layer seems to look far thinner than the actual thickness because of the similar secondary electron release property

between repeated two layers, although a certain amount of TiO_2 was included in hybrid SEO layer. It is thus worth noting that stabilization of BCP film by UV exposure induces the photo-crosslinking and this process is a crucial factor to prevent segmental mobility or solubility of the BCP film during consecutive adsorption. The distinct and representative advantage of this process is the aspect that BCP-based 1D structure having manifold inner architectures and compositions can be formed. The hybrid layered BCP structures containing silver nanoparticles as inorganic component were also fabricated in the same manner and their optical property was also compared (refer to supporting information).

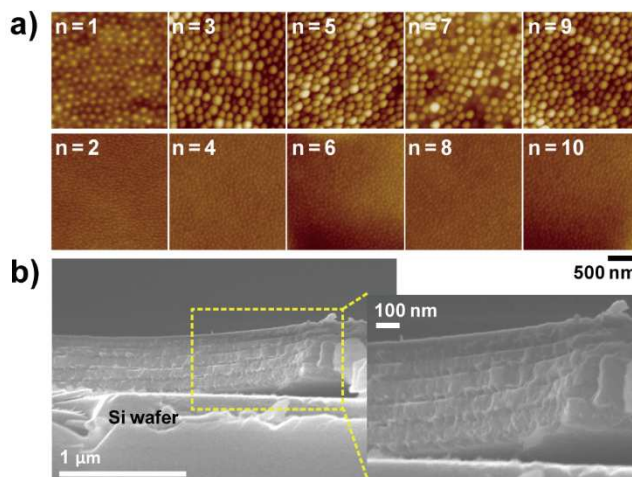


Fig. 1 a) AFM height surface morphologies of layered BCP films composed of S4VP(1%) (Upper part) and SEO/ TiO_2 (lower part) alternating layers (n is number of layer). b) Cross-sectional SEM images of ten-layered BCP structure: [S4VP(1%)/(SEO/ TiO_2)]₁₀.

On the basis of this procedure, 1D BCP-based layered structures having photonic band gap were obtained and their periodic size was tuned by controlling the inner architectures. To give rise to a difference in the refractive index of each layer, high volume contents of TiO_2 sol-gel precursors were included in SEO layer. The SEO layer with 40 vol% TiO_2 sol-gel precursor was used as the high refractive index layer ($n \approx 1.8$) and pristine S4VP layer was used as the low refractive index layer ($n \approx 1.64$). Appropriate thickness of each layer was simply tuned ranging from tens to hundreds of nanometers depending on the concentration of solution and rate of spin coating. Thickness of pure S4VP layer was adjusted by varying the concentrations of polymer solution and the values obtained from 1 wt% and 2 wt% solutions were about 36 nm and 78 nm, respectively. Thickness of SEO/ TiO_2 layer was set about 80 nm in a certain condition (such as particular volume fraction of TiO_2 sol-gel and spin speed). With refractive index (n) and proper thickness (d) of each layer, Bragg reflectance peak (λ_{max}) can be easily estimated according to following equation (1).

$$\lambda_{\text{max}} = 2(n_1d_1 + n_2d_2) \quad (1)$$

The calculated λ_{max} was 406 nm for BCP layered structures composed of 1 wt% S4VP and SEO/TiO₂ repetition layers. To evaluate the reflectivity of film, transmittance spectra were measured (Fig. 2). As predicted, transmission dip appeared around 410 nm correspond to the Bragg peak (Fig. 2(a)). When the number of stacked layers increases, transmission dip becomes more intense and is clearly seen due to the proper optical thickness between the higher and lower-index layers. The tuning of specific wavelength of transmission dips with respect to Bragg reflectance peak can be realized by changing the periodicity of the periodic multilayer. Keeping the conditions of SEO/TiO₂ layer the same, the concentration of S4VP solution was increased from 1 wt% to 2 wt%. It is observed that the transmission dip was red-shifted to around 540 nm as shown in Fig. 2(b), which complies with above mentioned equation. The stepwise layer-by-layer fabrication method for the stabilized BCP multilayers might be a promising way to fabricate 1D photonic structure with flexible stop bands in the whole wavelength ranges.

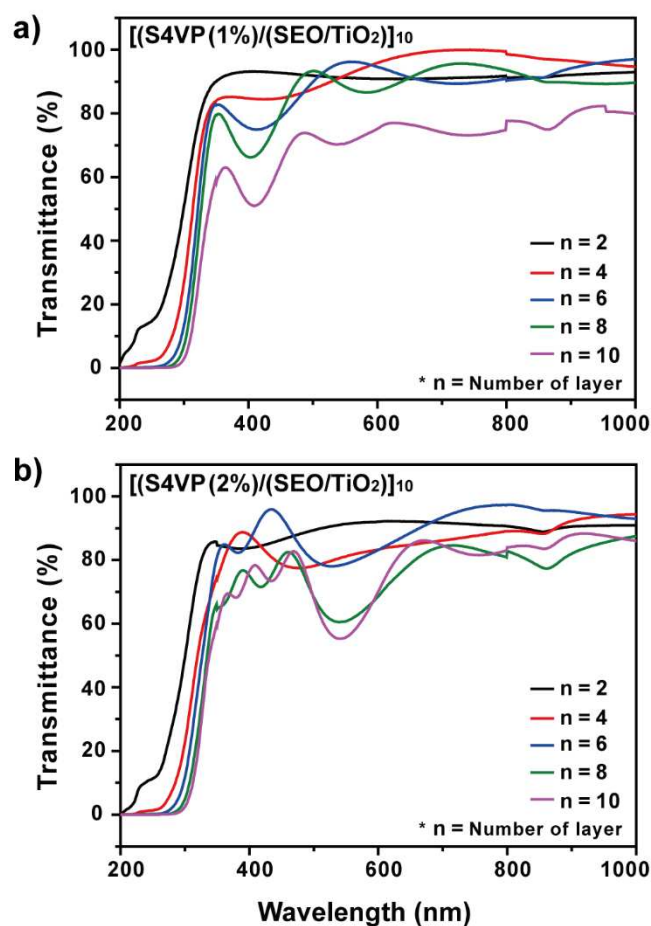


Fig. 2 Transmittance spectra of 1D BCP photonic structures composed of a) [S4VP(1%)/(SEO/TiO₂)]₁₀ and b) [S4VP(2%)/(SEO/TiO₂)]₁₀.

In terms of the organization of high-index SEO/TiO₂ layer, SEO polymer may give rise to lower the refractive index of the layer compared to pure TiO₂ ($n \approx 2.4$). A comparative experimental study was carried out by depositing the pure TiO₂

layer onto organic S4VP layer instead of SEO/TiO₂ layer. The thickness of the pure TiO₂ layer, for the desired λ_{max} , was adjusted to ~ 40 nm by controlling the spin speed and concentration of sol-gel precursors. The formation of Bragg stack layers consisting of S4VP (1%) and TiO₂ is assessed by the cross-sectional SEM image (inset of Fig. 3). The inorganic TiO₂ layer was clearly distinct from organic S4VP layer due to the high index contrast between the two alternating layers. When the thickness of organic layer was adjusted to ~ 80 nm, which was obtained from 2 wt% solution of S4VP polymer, transmission dip was observed at around 450 nm, which corresponds to calculated λ_{max} (Fig. 3). This result indicates that organic/inorganic Bragg stack having visible stop band can be realized. Importantly, it is noted that the relatively low-index hybrid organic/TiO₂ (*i.e.*, SEO/TiO₂) layer on behalf of pure TiO₂ also sufficiently manifests the photonic band gap in Bragg stack.

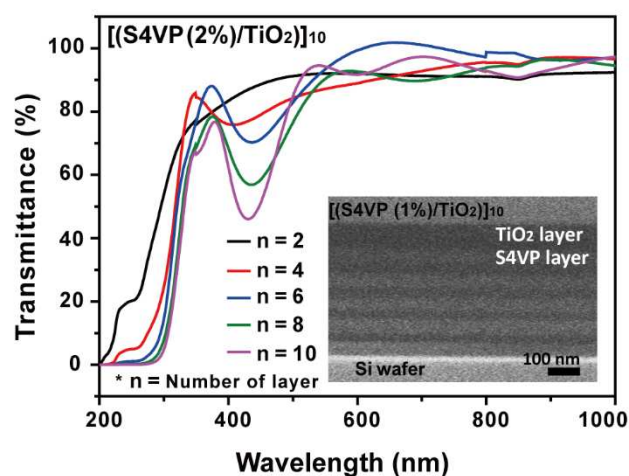
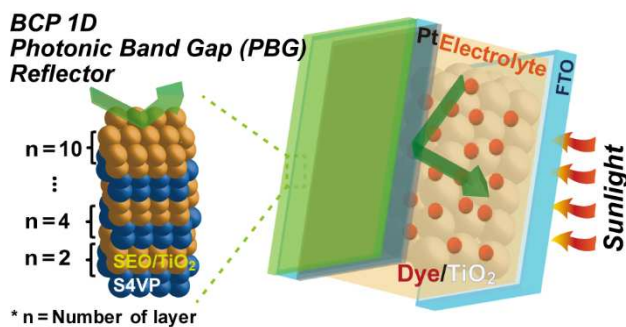


Fig. 3 Transmittance spectra of 1D Bragg stack layers composed of [S4VP(2%)/TiO₂]₁₀ (Inset: Cross-sectional SEM image of ten-layered Bragg stack structure [S4VP(1%)/TiO₂]₁₀).

The multilayered BCP films described above were introduced into the back-side of the counter electrodes in DSSCs to demonstrate the light reflection property of multilayered BCP films depending on their photonic stop bands. The photographs of the Pt coated FTO with and without BCP 1D photonic structures are provided in Fig. 4(a). The multilayered BCP films show the characteristic reflective colors and transmission dips were also clearly observed on the back-side of FTO (Fig. 4), which suggests that the BCP 1D photonic structure with appropriate thickness and periodicity can be used as light reflector in DSSCs to increase the light harvesting capability. Scheme 2 illustrates the configuration of DSSCs: N719 dye-sensitized nc-TiO₂ film as working electrode and Pt-coated FTO containing ten-layers of BCP 1D photonic band gap structures (Pt/FTO/PBG) at the other side of counter electrodes were assembled, and then iodide/triiodide redox couple were injected as hole transporter. The performances of the DSSCs equipped with different counter electrodes were measured under simulated sunlight with an illumination

intensity of 100 mW/cm^2 . The other parameters such as thickness of nc-TiO₂ film ($\sim 4 \mu\text{m}$), sputtered Pt ($\sim 2.8 \text{ nm}$), photo active area (0.25 cm^2), and cell assembly conditions were fixed to investigate the effect of the light reflection by PBG structures. Although the overall efficiency of the devices investigated in this study was relatively low, to maximize the light reflection effect, thin nc-TiO₂ film was used instead of thicker one that may absorb the most of the incoming light.



Scheme 2. Configuration of dye-sensitized solar cells containing BCP 1D photonic band gap (PBG) structures at back-side (non-conducting side) of counter electrode.

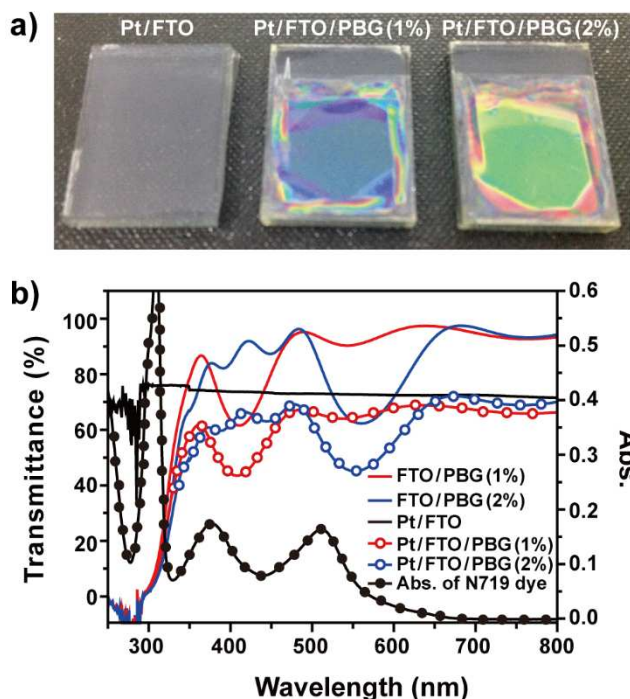


Fig. 4 a) photographs of counter electrodes: Pt/FTO, Pt/FTO/PBG (1%), Pt/FTO/PBG (2%). b) Transmittance spectra of 1D PBG structures on back-side of FTO substrate with or without Pt layer (left axis) and absorption spectrum of N719 dye molecules (right axis).

Fig. 5 shows the current density versus voltage (J - V) characteristic curve for three different devices and values of corresponding photovoltaic parameters (open-circuit voltage (V_{oc}), short-circuit current density (J_{sc}), fill factor (FF), and overall conversion efficiency (η)) were summarized in Table 1. As shown in the cell characteristics, V_{oc} and FF exhibit similar

values while J_{sc} was significantly increased for the case of PBG attached to counter electrode. It is interesting note that J_{sc} was systematically increased with increasing the periodic size of PBG structures, leading to an enhancement in power conversion efficiency. In the case of Pt/FTO/PBG (2%), the noticeable enhancement in J_{sc} is probably caused by better match between wavelength of dye absorption ranging from 500 to 600 nm and that of reflected light by PBG (2%) structures (Fig. 4(b)). Consequently, J_{sc} and efficiency reach its maximum enhancement 10.7 % and 10.9 % with respect to a cell with pristine Pt counter electrodes, respectively. It is worth noting that the enhanced J_{sc} can be attributed to the additional contribution of reflected light from layered 1D PBG structures, leading to an increase in the number of effective photons for electron-hole generation by dye molecules.

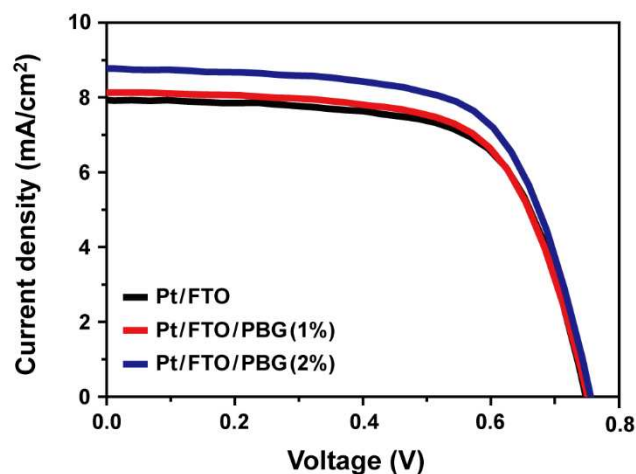


Fig. 5 J - V characteristic curves for three different counter electrodes: Pt/FTO, Pt/FTO/PBG (1%), Pt/FTO/PBG (2%).

Table 1. Summary of the photovoltaic parameters of DSSCs with different configurations of counter electrode.

Sample [a]	V_{oc} (V)	J_{sc} (mA/cm^2)	FF	η (%)
Pt/FTO	0.745 (± 0.003)	7.96 (± 0.04)	66.8 (± 0.19)	3.96 (± 0.02)
Pt/FTO/PBG (1%)	0.746 (± 0.005)	8.18 (± 0.06)	66.3 (± 0.38)	4.04 (± 0.02)
Pt/FTO/PBG (2%)	0.751 (± 0.005)	8.80 (± 0.07)	66.3 (± 0.23)	4.37 (± 0.01)

[a] Average over a large number of cells (more than 5-7 cells) for three kinds of counter electrode.

In order to prove that photocurrent improvement is caused by the effective utilization of incoming light via PBG multilayer, incident photon-to-current efficiency (IPCE) measurement was performed. As shown in Fig. 6(a), DSSCs containing PBG attached to counter electrode, specifically Pt/FTO/PBG (2%) counter electrode, exhibit higher IPCE than the control device with pristine Pt counter electrode over the whole wavelength range. The IPCE enhancement ratio ($\Delta\text{IPCE}/\text{IPCE}$, %) of PBG structures coupled DSSCs with respect to normal DSSCs clearly shows that wavelength-

dependent enhancement corresponds well with reflection wavelength of photonic structures (Fig. 6(b)). The relatively weak IPCE enhancement of the DSSCs composed of Pt/FTO/PBG (1%) counter electrode is mainly observed in the range 350 ~ 450 nm with a peak around 400 nm, which accords with maximum reflection of PBG (1%) structures. On the other hand, DSSCs composed of Pt/FTO/PBG (2%) counter electrode shows marked IPCE enhancement in the range of 500 ~ 600 nm as well as lower wavelength region (350 ~ 400 nm), which is most consistent with reflection feature of PBG (2%) structures as shown in Fig. 4(b). Incidentally, the enhancement at longer wavelength (above 600 nm) could be a manifestation of the poor signal-to-noise ratio in this spectral region. From IPCE measurement, it is concluded that the photocurrent improvement in DSSCs consisting of the PBG attached counter electrode might be attributed to the increased dye absorption by reflected light.

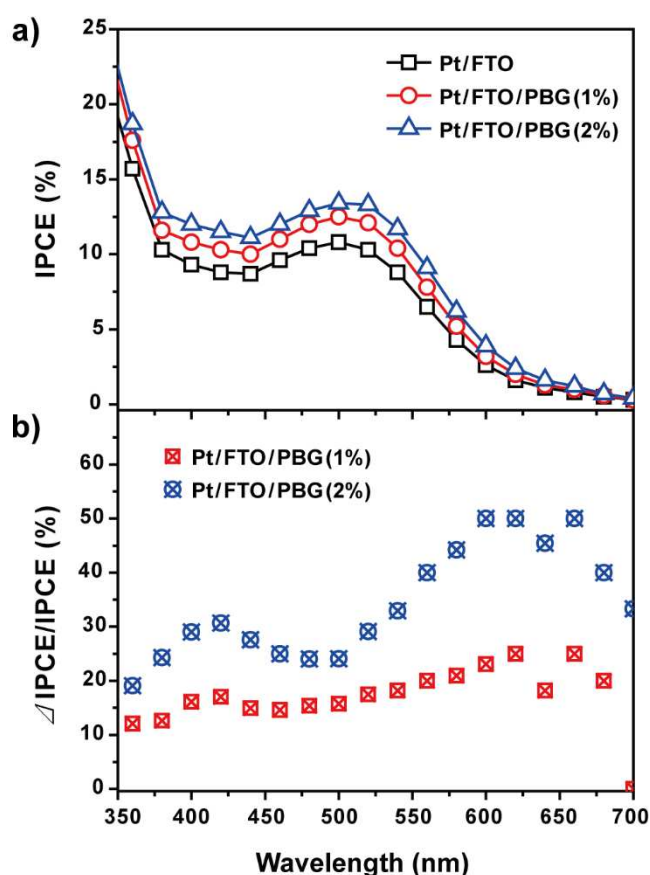


Fig. 6 a) IPCE curves for three different counter electrodes: Pt/FTO, Pt/FTO/PBG (1%), Pt/FTO/PBG (2%). b) IPCE enhancement ratio (Δ IPCE/IPCE, %) of DSSCs with Pt/FTO/PBG counter electrode with respect to DSSCs with pristine Pt counter electrode. Δ IPCE/IPCE (%) = (IPCE_{DSSCs with Pt/FTO/PBG counter electrode}(λ) - IPCE_{DSSCs with Pt/FTO counter electrode}(λ)) / (IPCE_{DSSCs with Pt/FTO counter electrode}(λ)) X 100 (%).

Considering the adsorption of dye molecules onto TiO₂ NPs, the lower porosity of the current polymer-based 1D photonic structures compared with inorganic-based 1D Bragg stacks or opal structures can be the main structural limitation or detrimental problem in coupling the PBG layer directly onto the

TiO₂ photoanode. To circumvent this, the PBG layer was introduced into the counter electrode and such a configuration may lead to optical losses caused by the electrolyte and Pt layer. This is a critical issue for the back reflection of light to maximize the light harvesting. However, Lee *et al.* recently reported that an inorganic-based Bragg stack layer was deposited onto the non-conducting side of the counter electrode to eliminate the disadvantages associated with direct deposition onto photoanodes.²⁶ The dense Bragg stack configured by alternating mesoporous TiO₂ and colloidal SiO₂ layers incorporated onto TiO₂ photoanode hinders the complete infiltration of electrolyte and increases the resistance throughout the cell, thereby resulting in significantly smaller V_{oc} and FF compared to DSSCs equipped with Bragg stack functionalized counter electrodes. On the other hand, it is interesting to note that similar enhancement of photocurrent was observed for both types of DSSCs. Thus, sufficient amount of light could be reflected by Bragg stack layer deposited on the rear surface of counter electrode and the LHE was increased although optical losses occurred.

Conclusions

In conclusion, we have demonstrated the synergistic effect of a new class of 1D PBG structures as light reflection layer in DSSCs, where the 1D layered structures were fabricated via BCP-based layer-by-layer self-assembly process. Successive alternating stacking of S4VP and SEO/TiO₂ layers were achieved by UV-stabilization in between the deposition of each layer. These multilayered BCP films have tailored specific photonic stop bands by simply controlling the periodic lattice parameter. The BCP 1D PBG structure was simply introduced into the counter electrodes as light reflector, and thus-fabricated cell efficiency was improved. For DSSCs containing PBG structure composed of S4VP (2%) and SEO/TiO₂ layers at the counter electrode, an enhancement by up to 11 % in the overall PCE was achieved compared with reference devices, which is comparable with the degree of efficiency enhancement induced by conventional inorganic-based PBG structures. Such an enhancement was mainly ascribed to the increased light harvesting by dye, which was arising from light reflection effects of BCP-based hybrid PBG structures at specific wavelength. Furthermore, we note that, this approach can be generalized and applied to other optical sensory device and energy devices by easily changing the inner architectures and compositions.

Acknowledgements

The authors thank Mr. Jaeyoon Park and Prof. Unyong Jeong at Yonsei University for the measurement of film thicknesses, Mr. Ho Yeon Kim and Prof. Du Yeol Ryu at Yonsei University for the measurement of reflective index, and Prof. Kyungkon Kim at Ewha Womans University for IPCE measurements. The authors specially thank Dr. Myunghwan Byun and Prof. Zhiqun Lin at Georgia Institute of Technology and Prof. Jun Hyuk Moon at Sogang University for fruitful discussions. This work was supported by the National Research Foundation (NRF) of

Korea Grant funded by the Korean Government (2011-0030255; 2011-0029409).

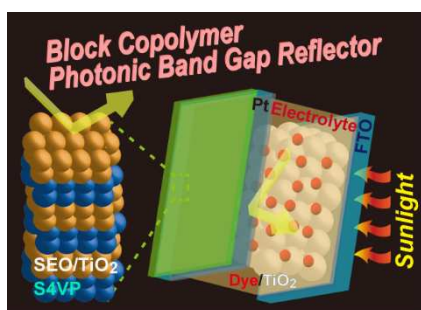
Notes and references

Department of Chemistry, Global Top 5 Research Program, Ewha Womans University, 52, Ewhayeodae-gil, Seodaemun-gu, Seoul, 120-750, South Korea.

† Electronic Supplementary Information (ESI) available: The characterization of hybrid layered BCP structures composed of S2VP and S4VP/Ag alternating layers is included. See DOI: 10.1039/b000000x/

- 1 B. O'Regan and M. Grätzel, *Nature*, 1991, **353**, 737.
- 2 M. Grätzel, *J. Photochem. Photobiol. C: Photochem. Rev.*, 2003, **4**, 145.
- 3 M. Grätzel, *Inorg. Chem.*, 2005, **44**, 6841.
- 4 M. Grätzel, *Acc. Chem. Res.*, 2009, **42**, 1788.
- 5 H. M. Upadhyaya, S. Senthilarasu, M.-H. Hsu and D. K. Kumar, *Sol. Energy Mat. Sol. Cells*, 2013, **119**, 291.
- 6 J. Burschka, N. Pellet, S.-J. Moon, R. Humphry-Baker, P. Gao, M. K. Nazeeruddin and M. Grätzel, *Nature*, 2013, **499**, 316.
- 7 S. Hore, C. Vetter, R. Kern, H. Smit and A. Hinsch, *Sol. Energy Mat. Sol. Cells*, 2006, **90**, 1176.
- 8 S. Ito, S. M. Zakeeruddin, R. Humphry-Baker, P. Liska, R. Charvet, P. Comte, M. K. Nazeeruddin, P. Péchy, M. Takata, H. Miura, S. Uchida and M. Grätzel, *Adv. Mater.*, 2006, **18**, 1202.
- 9 S.-H. Han, S. Lee, H. Shin and H. Suk Jung, *Adv. Energy Mater.*, 2011, **1**, 546.
- 10 M. Ye, D. Zheng, M. Lv, C. Chen, C. Lin and Z. Lin, *Adv. Mater.*, 2013, **25**, 3039.
- 11 X. Xin, H.-Y. Liu, M. Ye and Z. Lin, *Nanoscale*, 2013, **5**, 11220.
- 12 M. Ye, H. Y. Liu, C. Lin and Z. Lin, *Small*, 2013, **9**, 312.
- 13 M. D. Brown, T. Suteewong, R. S. S. Kumar, V. D'Innocenzo, A. Petrozza, M. M. Lee, U. Wiesner and H. J. Snaith, *Nano Lett.*, 2010, **11**, 438.
- 14 J. Qi, X. Dang, P. T. Hammond and A. M. Belcher, *ACS Nano*, 2011, **5**, 7108.
- 15 B. Ding, B. J. Lee, M. Yang, H. S. Jung and J.-K. Lee, *Adv. Energy Mater.*, 2011, **1**, 415.
- 16 Y. H. Jang, Y. J. Jang, S. T. Kochuveedu, M. Byun, Z. Lin and D. H. Kim, *Nanoscale*, 2014, DOI: 10.1039/c3nr05012b.
- 17 Y.-C. Lee, C.-F. Huang, J.-Y. Chang and M.-L. Wu, *Opt. Express*, 2008, **16**, 7969.
- 18 A. Čampa, J. Krč, F. Smole and M. Topič, *Thin Solid Films*, 2008, **516**, 6963.
- 19 S. Nishimura, N. Abrams, B. A. Lewis, L. I. Halaoui, T. E. Mallouk, K. D. Benkstein, J. van de Lagemaat and A. J. Frank, *J. Am. Chem. Soc.*, 2003, **125**, 6306.
- 20 Y. Zhang, J. Wang, Y. Zhao, J. Zhai, L. Jiang, Y. Song and D. Zhu, *J. Mater. Chem.*, 2008, **18**, 2650.
- 21 J. Y. Lee, S. Lee, J.-K. Park, Y. Jun, Y.-G. Lee, K. M. Kim, J. H. Yun and K. Y. Cho, *Opt. Express*, 2010, **18**, A522.
- 22 S. Colodrero, A. Forneli, C. López-López, L. Pellejà, H. Míguez and E. Palomares, *Adv. Funct. Mater.*, 2012, **22**, 1303.
- 23 S. Colodrero, A. Mihi, L. Häggman, M. Ocaña, G. Boschloo, A. Hagfeldt and H. Míguez, *Adv. Mater.*, 2009, **21**, 764.
- 24 S. Guldin, S. Hüttner, M. Kolle, M. E. Welland, P. Müller-Buschbaum, R. H. Friend, U. Steiner and N. Tétreault, *Nano Lett.*, 2010, **10**, 2303.
- 25 M. Guo, K. Xie, J. Lin, Z. Yong, C. T. Yip, L. Zhou, Y. Wang and H. Huang, *Energy Environ. Sci.*, 2012, **5**, 9881.
- 26 J. T. Park, J. H. Prosser, D. J. Kim, J. H. Kim and D. Lee, *ChemSusChem*, 2013, **6**, 856.
- 27 I. W. Hamley, *The Physics of Block Copolymers*, Oxford University Press, Oxford, 1998.
- 28 N. Hadjichristidis, S. Pispas and G. Floudas, *Block Copolymers: Synthetic Strategies, Physical Properties, and Applications*, John Wiley & Sons, Inc., 2003.
- 29 I. W. Hamley, *Developments in Block Copolymer Science and Technology*, John Wiley & Sons, Inc., 2004.
- 30 C. Kang, E. Kim, H. Baek, K. Hwang, D. Kwak, Y. Kang and E. L. Thomas, *J. Am. Chem. Soc.*, 2009, **131**, 7538.
- 31 M.-A. Cha, C. Shin, D. Kannaiyan, Y. H. Jang, S. T. Kochuveedu and D. H. Kim, *J. Mater. Chem.*, 2009, **19**, 7245.
- 32 S. Ito, P. Chen, P. Comte, M. K. Nazeeruddin, P. Liska, P. Pečny and M. Grätzel, *Prog. Photovolt: Res. Appl.*, 2007, **15**, 603.
- 33 Y. Wang, J. Liu, S. Christiansen, D. H. Kim, U. Gösele and M. Steinhart, *Nano Lett.*, 2008, **8**, 3993.
- 34 Y. H. Jang, S. T. Kochuveedu, Y. J. Jang, H. Y. Shin, S. Yoon, M. Steinhart and D. H. Kim, *Carbon*, 2011, **49**, 2120.
- 35 Y. H. Jang, X. Xin, M. Byun, Y. J. Jang, Z. Lin and D. H. Kim, *Nano Lett.*, 2012, **12**, 479.

Table of Contents



The block copolymer-based photonic structures are coupled into the counter electrodes as light reflector in dye-sensitized solar cells to increase the light harvesting.
